J. Phys. B: At. Mol. Opt. Phys. **41** (2008) 095204 (7pp) doi:10.1088/0953-4075/41/9/095204

# Electron-impact ionization of singly-charged neon ions

**J Lecointre**[1], **J J Jureta**[1,2] **and P Defrance**[1]

[1] Université Catholique de Louvain, Département de Physique, unité PAMO, Chemin du Cyclotron 2, B-1348 Louvain-la-Neuve, Belgium
[2] Institute of Physics, PO Box 68, 11081, Belgrade, Serbia

Received 21 December 2007, in final form 11 March 2008
Published 22 April 2008
Online at stacks.iop.org/JPhysB/41/095204

**Abstract**
Absolute cross sections for electron-impact single and multiple ionization of $Ne^+$ leading to the formation of $Ne^{q+}$ ($q = 2$–5) are reported. The animated crossed beams method is applied in the energy range from the respective thresholds up to 2.5 keV. The maximum cross sections are found to be $(4.12 \pm 0.21) \times 10^{-17}$ cm$^2$, $(1.42 \pm 0.07) \times 10^{18}$ cm$^2$, $(2.57 \pm 0.14) \times 10^{-20}$ cm$^2$, $(8.78 \pm 0.54) \times 10^{-22}$ cm$^2$ for the multiply-charged products $Ne^{q+}$ ($q = 2$–5), respectively. The corresponding threshold energies are measured to be $(41.0 \pm 0.5)$ eV, $(105 \pm 1)$ eV, $(205 \pm 5)$ eV and $(345 \pm 15)$ eV. Present data are compared with available experimental and theoretical results.

## 1. Introduction

Large amounts of atomic data (spectroscopic and collisional) are required for modelling the structure and dynamics of high-temperature plasmas occurring both naturally in space and artificially in fusion devices (Märk and Dunn 1985, Botero and Stephens 1996). Electron-impact ionization is the main mechanism for ion formation in the plasma and it is one of the fundamental processes in atomic physics. For this reason, accurate values of electron-impact ionization cross sections are especially helpful to interpret the observation of various plasma parameters (Janev 1993). Among the atomic species, numerous investigations over many decades have been performed regarding the rare gases (Rejoub *et al* 2002 and references therein).

Neon being frequently introduced in tokamaks as a diagnostic element for probing fusion plasmas, experiments concerning electron interaction with $Ne^{k+}$ ($k = 4$–8) atomic ions have formerly been carried out in our laboratory (Duponchelle *et al* 1997). Absolute cross sections were presented for electron-impact single ionization of multiply-charged $Ne^{k+}$ ($k = 4$–8) and for double ionization of $Ne^{5+}$ and $Ne^{6+}$. In addition, Zambra *et al* (1994) reported on the first absolute cross section measurements for electron-impact double ionization of singly-charged $Ne^+$ ions.

The present paper reports on results of experimental investigations for single and multiple ionization of $Ne^+$,

$$Ne^+ + e^- \rightarrow Ne^{2+} + 2e^- \qquad \sigma_1 \qquad (1)$$

$$\rightarrow Ne^{3+} + 3e^- \qquad \sigma_2 \qquad (2)$$

$$\rightarrow Ne^{4+} + 4e^- \qquad \sigma_3 \qquad (3)$$

$$\rightarrow Ne^{5+} + 5e^- \qquad \sigma_4. \qquad (4)$$

In the following section, the experimental method and set-up are presented for the measurement of absolute cross sections. The last section is devoted to the discussion of the results obtained for reactions (1)–(4) for electron energies ranging from the thresholds up to 2.5 keV. $Ne^{6+}$ products have also been observed, but the determination of the total cross sections over the whole energy range has not been achieved because of the difficulty of measuring such small cross sections.

## 2. Apparatus and experimental method

In this experiment, the animated crossed electron–ion beam method is applied (Defrance *et al* 1981). Both the present apparatus and the experimental method have recently been described in detail (Lecointre *et al* 2006) and a brief outline is presented here.

In the apparatus, the fixed-energy atomic ion beam interacts with an electron beam whose energy may be tuned from a few electron volts (eV) up to 2.5 keV. Ions are extracted from an electron cyclotron resonance (ECR) ion source and accelerated up to 8 keV. The ion beam is selected by means of a double focusing 90° magnetic analyser, additionally focused

 

**Table 1.** Typical working conditions and estimated uncertainties (one standard deviation).

| Parameter | Typical value | Systematic uncertainty (%) | Statistical uncertainty (%) |
|---|---|---|---|
| Kinematic factor, $A$ (s mC$^{-2}$) | $6.4 \times 10^{-29}$ | 0.5 | – |
| Sweeping speed, $u$ (m s$^{-1}$) | 3.75 | 1.0 | 1.0 |
| Electron current, $I_e$ (mA) | 1–3 | 0.5 | 1.0 |
| $Ne^+$ ion current, $I_i$ (nA) | 100–300 | 0.5 | 1.0 |
| Detection dfficiency, $\gamma$ | 1 | 1 | – |
| (1): Fragment: $Ne^{2+}$ | | | |
| Counts ($K$)/Luminosity ($L$) ($10^{20}$ Hz cm$^{-2}$) | 10/8 | – | 0.1 |
| Cross section, $\sigma_1$ ($10^{-17}$ cm$^2$) | 4.1 | 1.7 | 1.7 |
| (2): Fragment: $Ne^{3+}$ | | | |
| Counts ($K$)/Luminosity ($L$) ($10^{20}$ Hz cm$^{-2}$) | 0.6/10 | – | 0.5 |
| Cross section, $\sigma_2$ ($10^{-18}$ cm$^2$) | 1.4 | 1.7 | 1.8 |
| (3): Fragment: $Ne^{4+}$ | | | |
| Counts ($K$)/Luminosity ($L$) ($10^{20}$ Hz cm$^{-2}$) | $2 \times 10^{-2}/2$ | – | 2.4 |
| Cross section, $\sigma_3$ ($10^{-20}$ cm$^2$) | 2.6 | 1.7 | 3.0 |
| (4): Fragment: $Ne^{5+}$ | | | |
| Counts ($K$)/Luminosity ($L$) ($10^{20}$ Hz cm$^{-2}$) | $1 \times 10^{-3}/50$ | – | 4.0 |
| Cross section, $\sigma_4$ ($10^{-22}$ cm$^2$) | 8.8 | 1.7 | 4.4 |

and purified by a 45° spherical electrostatic deflector. The ion beam is directed into the collision region where it crosses the ribbon-shaped electron beam at right angles. The pressure is kept below $1 \times 10^{-9}$ mbar in the collision chamber. Product ions are separated from the primary ion beam by means of a double focusing 90° magnetic analyser. The angular acceptance of the magnet is large enough to transmit all ions to the detector. Product ions are further deflected by a 90° electrostatic spherical deflector and they are finally directed onto a channeltron detector.

In collision experiments, the cross section $\sigma$ is proportional to the count rate $N$, the proportionality factor being the luminosity ($N = L\sigma$). In experiments where the particle beams interact under at right angles, the luminosity factor $L$ is (Defrance *et al* 1981)

$$L = \frac{\left(v_e^2 + v_i^2\right)^{1/2}}{v_e v_i q_i e^2} \frac{I_e I_i}{F}. \tag{5}$$

In this expression, $e$ and $qe$, $v_e$ and $v_i$, are the charges and velocities of electrons and ions, $I_e$ and $I_i$ are the electron and ion beam current intensities, respectively. $F$ is the effective height over which the beams interact (i.e. the form factor). The luminosity factor includes all the parameters allowing the determination of the cross section, except the count rate, so that it expresses the global sensitivity of the experimental set-up.

In the animated beam method (Defrance *et al* 1981), the electron beam is swept across the ion beam in a linear motion at a constant speed $u$. The total number of events $K$ produced during one complete electron beam movement is related to the cross section $\sigma$ by the following expression:

$$\sigma = \frac{v_e v_i q_i e^2 u K}{\left(v_e^2 + v_i^2\right)^{1/2} I_e I_i \gamma}, \tag{6}$$

where $\gamma$ is the detector efficiency. Assuming $m_i \ll m_e$, the true interaction energy $E$ (eV) is given by

$$E = V_e + \frac{m_e}{m_i}(q_i V_i - V_e), \tag{7}$$

where $V_e$ and $V_i$, $m_e$ and $m_i$ are the acceleration voltages and masses of electrons and ions, respectively. The electron energy is corrected for the contact potential.

The angular acceptance of the magnet analyser allows for the total transmission of product fragments. Typical working conditions, statistical and systematic uncertainties of experimental parameters are listed in table 1 (one standard deviation). The total uncertainty (90% confidence limit) is obtained as the quadratic sum of the statistical and systematic uncertainties at the cross section maximum. Total uncertainties are found to be 4.0%, 4.1%, 5.6% and 7.7% for $\sigma_1$, $\sigma_2$, $\sigma_3$ and $\sigma_4$, respectively.

## 3. Results and discussion

Absolute cross sections ($\sigma_1$–$\sigma_4$) for the formation of $Ne^{q+}$ products, $q$ = 2–5, are listed in table 2, together with the associated total uncertainties, and they are shown in figures 1–4. The electron energy range extends from their respective ionization thresholds up to 2500 eV. Observed energy thresholds are summarized in table 3 jointly with data of Bashkin and Stoner (1975) and with some published experimental results (e.g. Zambra *et al* 1994, Gstir *et al* 2002, Rosenstock *et al* 1977).

The absolute cross section $\sigma_1$ ($Ne^{2+}$ formation, figure 1) shows the maximum value of $(4.12 \pm 0.21) \times 10^{-17}$ cm$^2$ at 215.1 eV. The $Ne^{2+}$ appearance energy is observed to be $(41.0 \pm 0.5)$ eV, which coincides with the spectroscopic value (41.0 eV: $Ne^+(1s^2 2s^2 2p^5, {}^2P_{3/2}) \rightarrow Ne^{2+}(1s^2 2s^2 2p^4, {}^3P_2)$). The weak signal observed below the ionization threshold (down to 37.1 eV) could be attributed to the presence of $Ne^+$ formed in a metastable state, but these cross sections are too small (0.1% of the maximum) to be investigated in detail.

Gstir *et al* (2002) reported the results of the experimental determination of the appearance energy values for the formation of $Ne^{q+}$ ions ($q$ = 1–4), following electron-impact ionization of neutral Ne atoms, by using a high-resolution mass spectrometer. In the fitting procedure, these authors

**Table 2.** Total cross sections for $Ne^{q+}$ ($q = 2$–5) ions, together with the associated uncertainties (90% confidence limit).

| | (1): $Ne^{2+}$ ($10^{-17}$ cm$^2$) | | (2): $Ne^{3+}$ ($10^{-18}$ cm$^2$) | | (3): $Ne^{4+}$ ($10^{-20}$ cm$^2$) | | (4): $Ne^{5+}$ ($10^{-22}$ cm$^2$) | |
|---|---|---|---|---|---|---|---|---|
| $E$ (eV) | $\sigma_1$ | $\Delta\sigma_1$ | $\sigma_2$ | $\Delta\sigma_2$ | $\sigma_3$ | $\Delta\sigma_3$ | $\sigma_4$ | $\Delta\sigma_4$ |
| 37.1 | 0.0020 | 0.0003 | – | – | – | – | – | – |
| 39.1 | 0.0026 | 0.0003 | – | – | – | – | – | – |
| 40.1 | 0.0050 | 0.0004 | – | – | – | – | – | – |
| 41.1 | 0.026 | 0.001 | – | – | – | – | – | – |
| 42.1 | 0.09 | 0.01 | – | – | – | – | – | – |
| 45.1 | 0.27 | 0.02 | – | – | – | – | – | – |
| 50.1 | 0.56 | 0.03 | – | – | – | – | – | – |
| 55.1 | 0.91 | 0.05 | – | – | – | – | – | – |
| 65.1 | 1.55 | 0.08 | – | – | – | – | – | – |
| 75.1 | 2.15 | 0.11 | – | – | – | – | – | – |
| 85.1 | 2.65 | 0.13 | – | – | – | – | – | – |
| 95.1 | 3.05 | 0.15 | – | – | – | – | – | – |
| 95.1 | 3.05 | 0.15 | – | – | – | – | – | – |
| 105.1 | – | – | 0.002 | 0.002 | – | – | – | – |
| 110.1 | – | – | 0.026 | 0.002 | – | – | – | – |
| 115.1 | 3.61 | 0.18 | 0.056 | 0.003 | – | – | – | – |
| 120.1 | – | – | 0.10 | 0.01 | – | – | – | – |
| 135.1 | 3.91 | 0.20 | 0.27 | 0.01 | – | – | – | – |
| 155.1 | 4.05 | 0.20 | 0.54 | 0.03 | – | – | – | – |
| 175.1 | 4.11 | 0.21 | 0.86 | 0.04 | – | – | – | – |
| 195.1 | 4.12 | 0.21 | 1.03 | 0.05 | – | – | – | – |
| 205.1 | – | – | – | – | 0.00 | 0.02 | – | – |
| 215.1 | 4.12 | 0.21 | 1.10 | 0.06 | 0.04 | 0.03 | – | – |
| 225.1 | – | – | – | – | 0.05 | 0.02 | – | – |
| 235.1 | 4.08 | 0.20 | | | 0.18 | 0.03 | – | – |
| 245.1 | – | – | 1.25 | 0.06 | 0.24 | 0.03 | – | – |
| 255.1 | 4.05 | 0.20 | – | – | 0.38 | 0.02 | – | – |
| 275.1 | – | – | – | – | 0.65 | 0.04 | – | – |
| 295.1 | 3.98 | 0.20 | 1.36 | 0.07 | 0.97 | 0.06 | – | – |
| 325.1 | – | – | – | – | 1.41 | 0.08 | – | – |
| 345.1 | – | – | 1.39 | 0.07 | 1.68 | 0.09 | 0.12 | 0.45 |
| 395.1 | 3.69 | 0.18 | 1.42 | 0.07 | 2.15 | 0.12 | 0.29 | 0.18 |
| 445.1 | – | – | 1.37 | 0.07 | 2.46 | 0.14 | 0.49 | 0.22 |
| 495.1 | 3.42 | 0.17 | 1.28 | 0.06 | 2.57 | 0.14 | 1.10 | 0.45 |
| 545.1 | – | – | – | – | 2.52 | 0.14 | – | – |
| 595.1 | 3.15 | 0.16 | 1.09 | 0.05 | 2.48 | 0.13 | 1.61 | 0.31 |
| 695.1 | – | – | – | – | 2.28 | 0.12 | 2.40 | 0.33 |
| 795.1 | 2.69 | 0.13 | 0.88 | 0.04 | 2.10 | 0.12 | 2.42 | 0.37 |
| 895.1 | – | – | – | – | 1.98 | 0.10 | 2.21 | 0.33 |
| 945.1 | – | – | – | – | 1.93 | 0.10 | – | – |
| 995.1 | 2.40 | 0.12 | 0.73 | 0.04 | 1.88 | 0.10 | 2.21 | 0.31 |
| 1095.1 | – | – | – | – | – | – | 2.70 | 0.39 |
| 1195.1 | – | – | – | – | 1.73 | 0.09 | 3.01 | 0.34 |
| 1345.1 | – | – | – | – | – | – | 4.53 | 0.40 |
| 1495.1 | 1.90 | 0.10 | 0.52 | 0.03 | 1.51 | 0.08 | 5.59 | 0.39 |
| 1795.1 | – | – | – | – | – | – | 7.15 | 0.54 |
| 1995.1 | 1.62 | 0.08 | 0.41 | 0.02 | 1.32 | 0.07 | 7.67 | 0.54 |
| 2195.1 | – | – | – | – | – | – | 7.83 | 0.54 |
| 2495.1 | 1.40 | 0.07 | 0.35 | 0.02 | 1.17 | 0.06 | 8.39 | 0.56 |
| 2795.1 | – | – | – | – | – | – | 8.78 | 0.54 |

applied the Marquart–Levenberg algorithm, with functions based on a Wannier-type power law, to describe the near-threshold behaviour of the cross section (Wannier 1955). The appearance energies were found in satisfactory agreement with the spectroscopic values of Rosenstock *et al* (1977). The Ne single ionization threshold (21.6 eV: $Ne(1s^22s^22p^6, {}^1S_0) \rightarrow Ne^+(1s^22s^22p^5, {}^2P_{3/2})$; Bashkin and Stoner 1975) is subtracted from the above-cited experimental values for comparison with present results. Excellent accordance is observed between all sets of data (table 3).

There is an overall general good agreement between the various experimental results available for $Ne^+$ single ionization cross sections. The observed discrepancies between these data may originate from experimental factors such as ion detection efficiency, transmission losses or ion source conditions (Bonham *et al* 1991, Bruce and Bonham 1992). In addition, primary ions may be formed in metastable states, which can affect the final result. Lennon *et al* (1988) recommended cross sections for electron-impact ionization reactions based on a critical compilation of both the experimental and the theoretical cross sections. The cross sections recommended

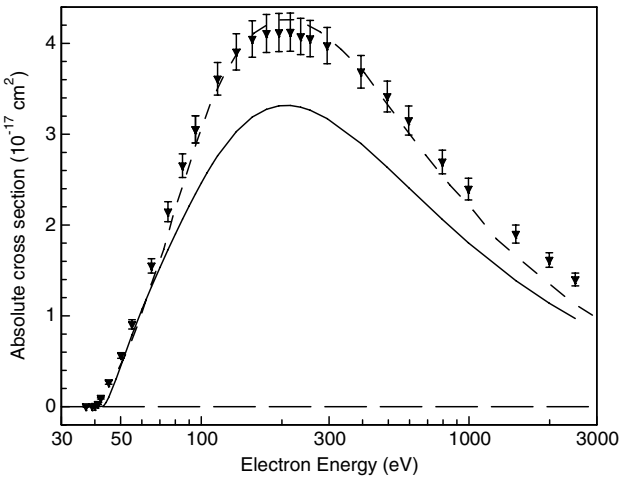


**Figure 1.** Cross sections for electron-impact single ionization ($\sigma_1$) of $Ne^+$ versus electron energy: (▼) present results; (—) recommended cross sections (Lennon *et al* 1988) and (– –) distorted-wave Born exchange approximation (Chongyang *et al* 1998).

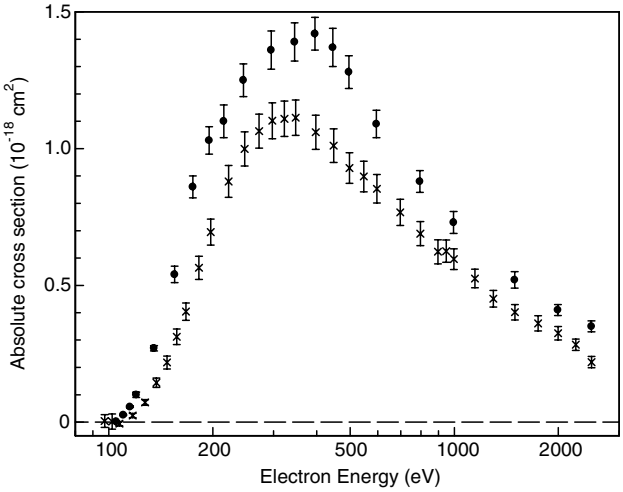


**Figure 2.** Cross sections for electron-impact double ionization of $Ne^+$ ($\sigma_2$) versus electron energy: (●) present results and (×) Zambra *et al* (1994).

for $Ne^+$ correspond to those measured by Diserens *et al* (1984) and agree closely with the high-energy Coulomb–Born results of Moores (1972). They underestimate present ones by about 20% around the maximum, but the agreement with present measurements improves in the low-energy region (figure 1). The observed difference is, in all probability, linked with the above-mentioned list of source of discrepancies. In particular, as pointed out above, a small signal below the threshold may indicate the presence of ions formed in metastable states. Chongyang *et al* (1998) applied the Distorted-wave-Born-exchange (DWBE) approximation to calculate $\sigma_1$. These results were observed to be in good accordance both with the DWBE results of Younger (1982), which are compiled by Tawara and Kato (1987), and with the Coulomb–Born-exchange (CBE) results of Moores (1972). All these Born-exchange results are in a fine agreement with present data over the whole energy range.

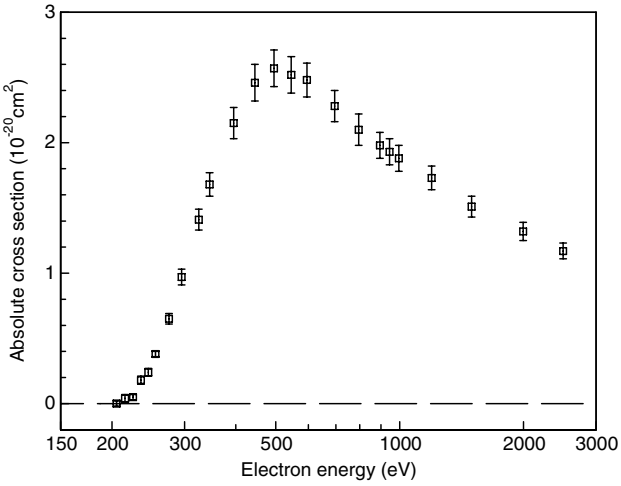


**Figure 3.** Cross sections for electron-impact triple ionization of $Ne^+$ (□, $\sigma_3$) versus electron energy.

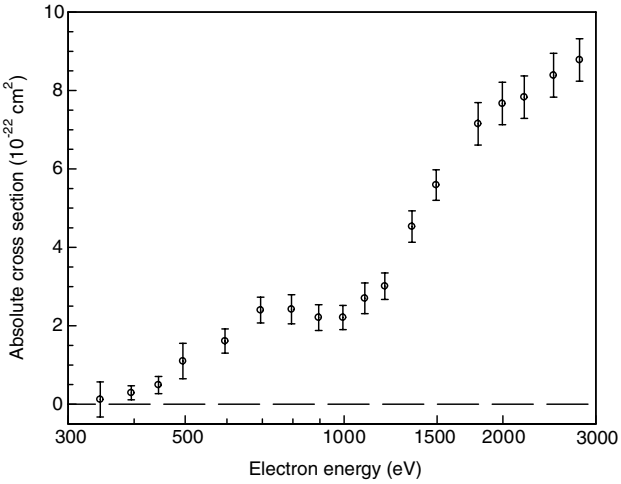


**Figure 4.** Cross sections for electron-impact quadruple ionization of $Ne^+$ (○, $\sigma_4$) versus electron energy.

**Table 3.** Threshold energies (eV) for the production of $Ne^{q+}$ fragments ($q = 2$–5).

| $e^- + Ne^+ \rightarrow$ | (1): $Ne^{2+}$ | (2): $Ne^{3+}$ | (3): $Ne^{4+}$ | (4): $Ne^{5+}$ |
|---|---|---|---|---|
| Present results | 41.0 ± 0.5 | 105 ± 1 | 205 ± 5 | 345 ± 15 |
| Bashkin and Stoner (1975) | 41.0 | 104.4 | 201.5 | 327.8 |
| Rosenstock *et al* (1977) | 41.0 | 104.4 | 201.5 | – |
| Gstir *et al* (2002) | 41.0 ± 0.2 | 104.2 ± 0.7 | 204.6 ± 4.7 | – |
| Zambra *et al* (1994) | – | 105 ± 2 | – | – |

The absolute cross section $\sigma_2$ ($Ne^{3+}$ formation, figure 2) exhibits the maximum value of $(1.42 \pm 0.07) \times 10^{-18}$ cm$^2$ at 395.1 eV. The $Ne^{3+}$ appearance energy, observed at (105 ±

**Table 4.** Fitting parameters of the Bethe-plots ($a$, $b$) and integrated oscillator strength ($M_n^2$) for each $Ne^{q+}$ fragment ($q = 2$–5). The parameter $a$ is expressed in $10^{-14}$ cm$^2$ eV$^2$, whereas $b$ and $M_n^2$ have no units.

| $e^- + Ne^+ \rightarrow$ | (1): $Ne^{2+}$ | (2): $Ne^{3+}$ | (3): $Ne^{4+}$ | (4): $Ne^{5+}$ |
|---|---|---|---|---|
| $a$ | $41.6 \pm 0.4$ | $2.21 \pm 0.02$ | $0.20 \pm 0.01$ | $0.080 \pm 0.005$ |
| $b$ | $-0.78 \pm 0.02$ | $1.15 \pm 0.03$ | $0.36 \pm 0.01$ | $-1.14 \pm 0.01$ |
| $M_n^2$ | $2.12 \pm 0.03$ | $(4.40 \pm 0.01) \times 10^{-2}$ | $(2.07 \pm 0.07) \times 10^{-3}$ | $(5.1 \pm 0.1) \times 10^{-4}$ |

1) eV, agrees perfectly both with experimental result (Gstir *et al* 2002) and with the spectroscopic value (104.4 eV: $Ne^+(1s^22s^22p^5, {}^2P_{3/2}) \rightarrow Ne^{3+}(1s^22s^22p^3, {}^4S_{3/2})$, Bashkin and Stoner 1975). Around the maximum, present cross sections are found to be 20% higher than the previous measurements of Zambra *et al* (1994), but they agree together in the threshold region. It is worth mentioning that this experiment was performed in our laboratory with different apparatus and different data analysis method. Therefore, the source of observed discrepancies between the two sets of data is also to be found in the above-presented list for single ionization.

The maximum absolute cross section $\sigma_3$ ($Ne^{4+}$ formation, figure 3) is measured to be $(2.57 \pm 0.14) \times 10^{-20}$ cm$^2$ at 495.1 eV. The $Ne^{4+}$ ionization potential is found to be $(205 \pm 5)$ eV, which perfectly agrees with the experimental value ($204.6 \pm 4.7$ eV) of Gstir *et al* (2002), although these values are found to be slightly higher than the spectroscopic one (201.5 eV: $Ne^+(1s^22s^22p^5, {}^2P_{3/2}) \rightarrow Ne^{4+}(1s^22s^22p^2, {}^3P_0)$).

The $Ne^{5+}$ appearance energy is affected by much larger uncertainty than lower charge states, due to the smallness of this cross section. The result ($345 \pm 15$ eV) is not incompatible with the spectroscopic energy (327.8 eV: $Ne^+(1s^22s^22p^5, {}^2P_{3/2}) \rightarrow Ne^{5+}(1s^22s^22p, {}^2P_{1/2})$). For $Ne^{5+}$, the absolute cross section $\sigma_4$ (figure 4) reaches a plateau (about $(2.4 \pm 0.3) \times 10^{-22}$ cm$^2$, at 700 eV) and, above $950 \pm 20$ eV, the cross section increases continuously up to $(8.8 \pm 0.5) \times 10^{-22}$ cm$^2$ at 2800 eV. Such a shape indicates the presence of Auger processes resulting from ejection of one electron belonging to the $Ne^+$ K-shell of whom binding energy is determined to be 914.6 eV (Clementi and Roetti 1974). Keeping in mind the high uncertainty associated with the observed result, this foreseen value is comparable with the present one. Contributions from K-shell ionization are usually neglected in theoretical calculations. For $Ne^+$ (e.g. Lotz 1968), this contribution is estimated to be of the order of $4 \times 10^{-20}$ cm$^2$ around the maximum. This is much too small (less than a fraction of 1%) to be significantly observed in single and in double ionization (Man *et al* 1987). For triple ionization, the slope of high-energy cross sections could indicate some possible minor contribution of multiple auto-ionization following K-shell ionization. The analysis of the intricate cascade auto-ionization pathway should enlighten this process.

Finally, attempts to observe $Ne^{6+}$ products were successful and the cross section is found to be $(6.2 \pm 2.5) \times 10^{-23}$ cm$^2$ at 1995.1 eV incident electron energy. Nevertheless, the signal was too weak to measure total cross sections over the whole energy range, and to determine the appearance energy, which is predicted to be 485.7 eV ($Ne^+(1s^22s^22p^5, {}^2P_{3/2}) \rightarrow Ne^{6+}(1s^22s^2, {}^1S_0)$, Bashkin and Stoner 1975).

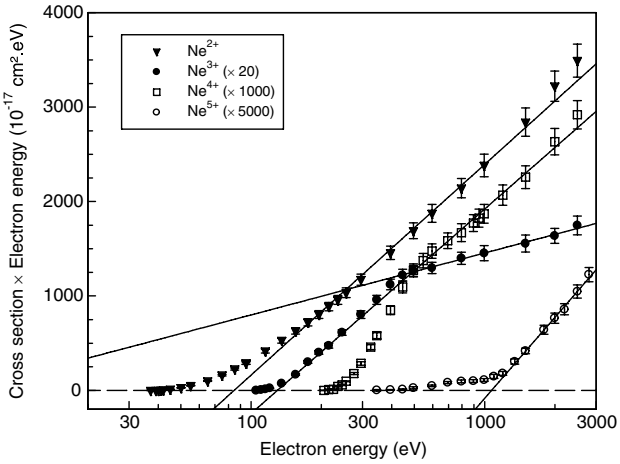


**Figure 5.** Bethe-plots of cross sections for $Ne^{q+}$ fragments ($q = 2$–5).

The Bethe-plot of present ionization cross sections shows that, in the high-energy region, the data are well adjusted along a straight line (figure 5). This shows that the energy dependence of the electron-impact ionization cross section can adequately be represented by the usual Bethe-form

$$\sigma_n = \frac{a}{E I_n}\left[\ln\left(\frac{E}{I_n}\right) + b\right], \tag{8}$$

where $a$ ($10^{-14}$ cm$^2$ eV$^2$) and $b$ are fitting parameters; $I_n$ (eV), $n = 1$–4, represents the threshold energy of reactions (1)–(4). The straight lines (figure 5) represent the result of the least-square fit of the cross sections (table 4). Moreover, the fitting parameter $a$ is directly related to the generalized oscillator strength $\left(M_n^2\right)$ (Inokuti 1971) as follows:

$$M_n^2 = \frac{a}{4\pi a_0^2 R I_n}, \tag{9}$$

where $a_0$ is the first Bohr radius of atomic hydrogen and $R$ is the Rydberg energy. The present $M_n^2$ values, which are calculated for each multiple ionization process (1)–(4), are also listed in table 4. Present oscillator strengths $\left(M_n^2\right)$ are comparable with the results acquired for electron-impact ionization of neon atoms. Oscillator strengths for single, double, triple and quadruple ionization of neutral neon are found to be $(2.06 \pm 0.31)$, $(4.6 \pm 1.7) \times 10^{-2}$, $(2.1 \pm 0.6) \times 10^{-3}$ and $(7.9 \pm 2.5) \times 10^{-4}$, respectively (Almeida *et al* 1995). For a given number of ejected electrons, the above-listed values are similar (within their combined error bars) to the present ones that were obtained for ionization of $Ne^+$ (table 4).

Different basic mechanisms lead to the production of multiply ionized species. The dominant ones are (i) direct

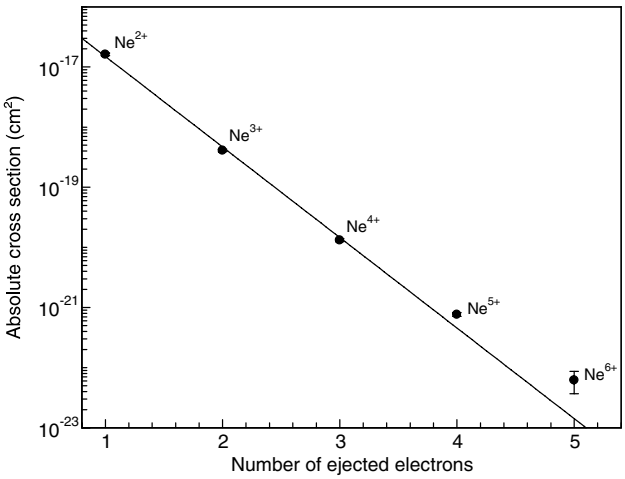


**Figure 6.** Ionization cross sections (•) plotted as a function of the number of ejected electrons for $E = 1995.1$ eV. The straight line results from the fitting procedure (equation (10)); the effective charge $q_0$ is calculated to be 0.288.

ejection of two or more electrons from the outer-shell by the impinging electron, (ii) shake-off mechanisms and (iii) ionization or excitation of an inner-shell electron followed by one or more Auger processes. The high-energy behaviour of the cross section, described by the Bethe–Born approximation, reflects the respective role of these mechanisms. For single ionization, the logarithmic term (in equation (8)) is known to be dominant, what corresponds to direct electron ejection, but for double ionization shake-off is supposed to be the dominant process. For triple ionization the logarithmic term and $b$ parameter (in equation (8)) are seen to be almost equivalent. For quadruple ionization, the Bethe-plot evidently confirms the role of K-shell ionization. In the low-energy region, that is, below the region of validity of the Bethe–Born approximation, the shape of various cross sections differs from each other, indicating competition between the above-described contributing mechanisms.

At a given electron energy, the cross sections are seen to reduce strongly with increasing charge state: for instance, at 1995.1 eV electron energy, $\sigma_2$, $\sigma_3$ and $\sigma_4$ are found to be 2.5%, 0.08% and 0.005% of $\sigma_1$, respectively. A search for the charge dependence of ionization cross sections (Tian and Vidal 1999) showed that, for molecules, the cross section behaviour is adequately reproduced via the following expression:

$$\sigma_n = \sigma_1 \times \exp\left[-\frac{(n-1)}{q_0}\right], \qquad (10)$$

where $n$ represents the number of ejected electrons of the ionic products $Ne^{q+}$ ($q = n + 1$), $\sigma_1$ (cm$^2$) is the single ionization cross section and the fitting parameter $q_0$ appears to be an effective charge. In a semi-log scale, the ionization cross sections exhibit a typical linear dependence versus the ionization stage. They are shown in figure 6, for the production of $Ne^{2+}$, $Ne^{3+}$, $Ne^{4+}$, $Ne^{5+}$ and $Ne^{6+}$, at $E = 1995.1$ eV. For each of the incident electron energies where processes (1)–(4) play a significant role, this particular exponential behaviour is established and accurately reproduced by the fitting function (10). The effective charge $q_0$ continuously increases from 0.242 up to 0.294, for electron energies ranging from $E = 395.1$ eV up to 2995.1 eV, respectively. Further theoretical investigations should bring a better understanding of such experimentally observed behaviour, which is related to the effective charges perceived by the ejected electrons and to their binding energies.

## 4. Summary

Absolute cross sections for electron-impact single and multiple ionization of $Ne^+$, leading to the formation of $Ne^{q+}$ ($q = 2$–5), are reported from the respective thresholds up to 2.5 keV. Appearance energies are found to be in satisfactory agreement with published data (e.g. Bashkin and Stoner 1975, Rosenstock *et al* 1977, Gstir *et al* 2002). For single and double ionization, present cross sections agree with available theoretical and experimental results. First results are achieved for triple and quadruple ionization. In the latter case, the cross section is seen to be dominated by Auger processes resulting from ejection of one electron belonging to the $Ne^+$ K-shell. The generalized oscillator strength is deduced from high-energy ionization cross sections. At a given incident electron energy, multiple ionization cross sections are observed to decrease exponentially with respect to the final ionization stage of products, which corroborates observations of Tian and Vidal (1999) obtained for molecules.

## Acknowledgments

Authors acknowledge the financial support of the Association Euratom-Belgian State and the technical support of C Alaime and D Dedouaire. They are indebted to the Forschungszentrum Jülich for the lending of the ECR ion source.

## References

Almeida D P, Fontes A C and Godinho C F L 1995 *J. Phys. B: At. Mol. Opt. Phys.* **28** 3335
Bashkin S and Stoner J O Jr 1975 *Atomic Energy Levels & Grotrian Diagrams I, Hydrogen I–Phosphorus XV* (Amsterdam: Elsevier)
Bonham R A, Bruce M R and Ma C 1991 *Collision Processes of Ion, Positron, Electron and Photon Beams in Matter* (Latin American School of Physics) (Singapore: World Scientific) p 329
Botero J and Stephens J A 1996 *Int. Bull. At. Mol. Data Fusion* 50–1
Bruce M R and Bonham R A 1992 *Z. Phys.* D **24** 149
Chongyang C, Shixiang Y, Zhouxuan T, Yansen W, Fujia Y and Yongsheng S 1998 *J. Phys. B: At. Mol. Opt. Phys.* **31** 2667
Clementi E and Roetti C 1974 *At. Data Nucl. Data Tables* **14** 177
Defrance P, Brouillard F, Claeys W and Van Wassenhove G 1981 *J. Phys. B: At. Mol. Phys.* **14** 103
Diserens M J, Harrison M F A and Smith A C H 1984 *J. Phys. B: At. Mol. Opt. Phys.* **17** L621
Duponchelle M, Khouilid M, Oualim E M, Zhang H and Defrance P 1997 *J. Phys. B: At. Mol. Opt. Phys.* **30** 729
Gstir B, Denifl S, Hanel G, Rümmele M, Fiegele T, Cicman P, Stano M, Matejcik S, Scheier P, Becker K, Stamatovic A and Märk T D 2002 *J. Phys. B: At. Mol. Opt. Phys.* **35** 2993
Inokuti M 1971 *Rev. Mod. Phys.* **43** 297

Janev R K Summary report of the IAEA technical committee meeting on atomic and molecular data for fusion reactor technology 1993 *Report* INDC (NDS-277) (Vienna: IAEA)
Lecointre J, Belic D S, Cherkani-Hassani H, Jureta J J and Defrance P 2006 *J. Phys. B: At. Mol. Opt. Phys.* **39** 3275
Lennon M A, Bell K L, Gilbody H B, Hughes J G, Kingston A E, Murray M J and Smith F J 1988 *J. Phys. Chem.* **17** 1285
Lotz W 1968 *Z. Phys.* **216** 241
Man K F, Smith A C H and Harrison M F A 1987 *J. Phys. B: At. Mol. Phys.* **20** 5865
Märk T D and Dunn G H 1985 *Electron-Impact Ionization* (Vienna: Springer)
Moores D L 1972 *J. Phys. B: At. Mol. Opt. Phys.* **5** 286
Rejoub R, Lindsay B G and Stebbings R F 2002 *Phys. Rev.* A **65** 042713
Rosenstock H M, Draxl K, Steiner B W and Herron J T 1977 Energetics of gaseous ions *J. Chem. Ref. Data* **6**
Tawara H and Kato T 1987 *At. Data Nucl. Data Tables* **36** 167
Tian C and Vidal C R 1999 *Phys. Rev.* A **59** 1955
Wannier G H 1955 *Phys. Rev.* **100** 1180
Younger S M 1982 Private communication (cited by Tawara *et al* 1987)
Zambra M, Belic D S, Defrance P and Yu D J 1994 *J. Phys. B: At. Mol. Opt. Phys.* **27** 2383